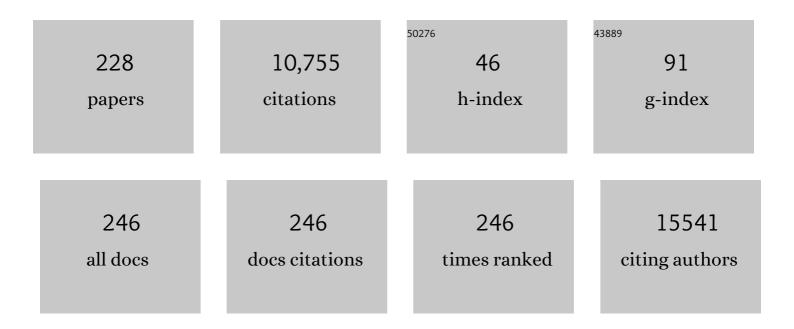
## Boudewijn P F Lelieveldt

List of Publications by Year in descending order

Source: https://exaly.com/author-pdf/1566515/publications.pdf Version: 2024-02-01



#	Article	IF	CITATIONS
1	Deep Recursive Embedding for High-Dimensional Data. IEEE Transactions on Visualization and Computer Graphics, 2022, 28, 1237-1248.	4.4	3
2	Fully Automated 3D Vestibular Schwannoma Segmentation with and without Gadolinium-based Contrast Material: A Multicenter, Multivendor Study. Radiology: Artificial Intelligence, 2022, 4, .	5.8	11
3	Visual cohort comparison for spatial single-cell omics-data. IEEE Transactions on Visualization and Computer Graphics, 2021, 27, 733-743.	4.4	13
4	ImaCytE: Visual Exploration of Cellular Micro-Environments for Imaging Mass Cytometry Data. IEEE Transactions on Visualization and Computer Graphics, 2021, 27, 98-110.	4.4	61
5	Evaluation of the Robustness of Learned MR Image Reconstruction to Systematic Deviations Between Training and Test Data for the Models from the fastMRI Challenge. Lecture Notes in Computer Science, 2021, , 25-34.	1.3	3
6	Hierarchical Prediction of Registration Misalignment Using a Convolutional LSTM: Application to Chest CT Scans. IEEE Access, 2021, 9, 62008-62020.	4.2	11
7	Iron loading is a prominent feature of activated microglia in Alzheimer's disease patients. Acta Neuropathologica Communications, 2021, 9, 27.	5.2	79
8	Systems analysis and controlled malaria infection in Europeans and Africans elucidate naturally acquired immunity. Nature Immunology, 2021, 22, 654-665.	14.5	24
9	A machine learning method for the discovery of minimum marker gene combinations for cell type identification from single-cell RNA sequencing. Genome Research, 2021, 31, 1767-1780.	5.5	50
10	Semiâ€automated background removal limits data loss and normalizes imaging mass cytometry data. Cytometry Part A: the Journal of the International Society for Analytical Cytology, 2021, 99, 1187-1197.	1.5	18
11	Comparative cellular analysis of motor cortex in human, marmoset and mouse. Nature, 2021, 598, 111-119.	27.8	361
12	Stochastic neighbor embedding as a tool for visualizing the encoding capability of magnetic resonance fingerprinting dictionaries. Magnetic Resonance Materials in Physics, Biology, and Medicine, 2021, , 1.	2.0	1
13	High-dimensional cytometric analysis of colorectal cancer reveals novel mediators of antitumour immunity. Gut, 2020, 69, 691-703.	12.1	92
14	GPGPU Linear Complexity t-SNE Optimization. IEEE Transactions on Visualization and Computer Graphics, 2020, 26, 1172-1181.	4.4	40
15	Deep Learning for Quantitative Cardiac MRI. American Journal of Roentgenology, 2020, 214, 529-535.	2.2	20
16	Helminth infections drive heterogeneity in human type 2 and regulatory cells. Science Translational Medicine, 2020, 12, .	12.4	33
17	Automatic coronary artery plaque thickness comparison between baseline and followâ€up CCTA images. Medical Physics, 2020, 47, 1083-1093.	3.0	4
18	Multidimensional analyses of proinsulin peptide-specific regulatory T cells induced by tolerogenic dendritic cells. Journal of Autoimmunity, 2020, 107, 102361.	6.5	7

## BOUDEWIJN P F LELIEVELDT

#	Article	IF	CITATIONS
19	A community-based transcriptomics classification and nomenclature of neocortical cell types. Nature Neuroscience, 2020, 23, 1456-1468.	14.8	183
20	An Adaptive Intelligence Algorithm for Undersampled Knee MRI Reconstruction. IEEE Access, 2020, 8, 204825-204838.	4.2	59
21	Eleven grand challenges in single-cell data science. Genome Biology, 2020, 21, 31.	8.8	742
22	SCHNEL: scalable clustering of high dimensional single-cell data. Bioinformatics, 2020, 36, i849-i856.	4.1	4
23	Focus+Context Exploration of Hierarchical Embeddings. Computer Graphics Forum, 2019, 38, 569-579.	3.0	5
24	Conserved cell types with divergent features in human versus mouse cortex. Nature, 2019, 573, 61-68.	27.8	1,198
25	Early-Life Compartmentalization of Immune Cells in Human Fetal Tissues Revealed by High-Dimensional Mass Cytometry. Frontiers in Immunology, 2019, 10, 1932.	4.8	15
26	Memory CD4+ T cells are generated in the human fetal intestine. Nature Immunology, 2019, 20, 301-312.	14.5	132
27	Quantitative error prediction of medical image registration using regression forests. Medical Image Analysis, 2019, 56, 110-121.	11.6	28
28	Quantification of aortic pulse wave velocity from a population based cohort: a fully automatic method. Journal of Cardiovascular Magnetic Resonance, 2019, 21, 27.	3.3	11
29	CyTOFmerge: integrating mass cytometry data across multiple panels. Bioinformatics, 2019, 35, 4063-4071.	4.1	23
30	An Efficient Preconditioner for Stochastic Gradient Descent Optimization of Image Registration. IEEE Transactions on Medical Imaging, 2019, 38, 2314-2325.	8.9	13
31	Evaluation of an Open Source Registration Package for Automatic Contour Propagation in Online Adaptive Intensity-Modulated Proton Therapy of Prostate Cancer. Frontiers in Oncology, 2019, 9, 1297.	2.8	5
32	A novel software tool for semi-automatic quantification of thoracic aorta dilatation on baseline and follow-up computed tomography angiography. International Journal of Cardiovascular Imaging, 2019, 35, 711-723.	1.5	17
33	A model-guided method for improving coronary artery tree extractions from CCTA images. International Journal of Computer Assisted Radiology and Surgery, 2019, 14, 373-383.	2.8	4
34	Interactive Visual Exploration of 3D Mass Spectrometry Imaging Data Using Hierarchical Stochastic Neighbor Embedding Reveals Spatiomolecular Structures at Full Data Resolution. Journal of Proteome Research, 2018, 17, 1054-1064.	3.7	37
35	Mass cytometry reveals innate lymphoid cell differentiation pathways in the human fetal intestine. Journal of Experimental Medicine, 2018, 215, 1383-1396.	8.5	74
36	Automatic quantification of bone marrow edema on <scp>MRI</scp> of the wrist in patients with early arthritis: A feasibility study. Magnetic Resonance in Medicine, 2018, 79, 1127-1134.	3.0	21

BOUDEWIJN P F LELIEVELDT

#	Article	IF	CITATIONS
37	CyteGuide: Visual Guidance for Hierarchical Single-Cell Analysis. IEEE Transactions on Visualization and Computer Graphics, 2018, 24, 739-748.	4.4	20
38	DeepEyes: Progressive Visual Analytics for Designing Deep Neural Networks. IEEE Transactions on Visualization and Computer Graphics, 2018, 24, 98-108.	4.4	121
39	A structural equation model for imaging genetics using spatial transcriptomics. Brain Informatics, 2018, 5, 13.	3.0	6
40	Integrating spatial-anatomical regularization and structure sparsity into SVM: Improving interpretation of Alzheimer's disease classification. NeuroImage, 2018, 178, 445-460.	4.2	49
41	Histogramâ€based standardization of intravascular optical coherence tomography images acquired from different imaging systems. Medical Physics, 2018, 45, 4158-4170.	3.0	1
42	Multiscale Visualization and Exploration of Large Bipartite Graphs. Computer Graphics Forum, 2018, 37, 549-560.	3.0	12
43	Heterogeneity of circulating CD8 T-cells specific to islet, neo-antigen and virus in patients with type 1 diabetes mellitus. PLoS ONE, 2018, 13, e0200818.	2.5	38
44	A quality score for coronary artery tree extraction results. , 2018, , .		2
45	Semi-automated Processing of Real-Time CMR Scans for Left Ventricle Segmentation. Lecture Notes in Computer Science, 2018, , 57-66.	1.3	0
46	Advanced two-layer level set with a soft distance constraint for dual surfaces segmentation in medical images. , 2018, , .		1
47	Approximated and User Steerable tSNE for Progressive Visual Analytics. IEEE Transactions on Visualization and Computer Graphics, 2017, 23, 1739-1752.	4.4	213
48	Toward optical guidance during endoscopic ultrasound-guided fine needle aspirations of pancreatic masses using single fiber reflectance spectroscopy: a feasibility study. Journal of Biomedical Optics, 2017, 22, 024001.	2.6	20
49	Fully-automatic left ventricular segmentation from long-axis cardiac cine MR scans. Medical Image Analysis, 2017, 39, 44-55.	11.6	23
50	Quantification of aortic annulus in computed tomography angiography: Validation of a fully automatic methodology. European Journal of Radiology, 2017, 93, 1-8.	2.6	12
51	BrainScope: interactive visual exploration of the spatial and temporal human brain transcriptome. Nucleic Acids Research, 2017, 45, gkx046.	14.5	29
52	Brain transcriptome atlases: a computational perspective. Brain Structure and Function, 2017, 222, 1557-1580.	2.3	19
53	An objective comparison of cell-tracking algorithms. Nature Methods, 2017, 14, 1141-1152.	19.0	399
54	Timing and localization of human dystrophin isoform expression provide insights into the cognitive phenotype of Duchenne muscular dystrophy. Scientific Reports, 2017, 7, 12575.	3.3	123

#	Article	IF	CITATIONS
55	Nonrigid Image Registration Using Multi-scale 3D Convolutional Neural Networks. Lecture Notes in Computer Science, 2017, , 232-239.	1.3	161
56	Visual analysis of mass cytometry data by hierarchical stochastic neighbour embedding reveals rare cell types. Nature Communications, 2017, 8, 1740.	12.8	198
57	Computer-aided evaluation of inflammatory changes over time on MRI of the spine in patients with suspected axial spondyloarthritis: a feasibility study. BMC Medical Imaging, 2017, 17, 55.	2.7	2
58	Automatic identification of coronary tree anatomy in coronary computed tomography angiography. International Journal of Cardiovascular Imaging, 2017, 33, 1809-1819.	1.5	29
59	Assessment of viscous energy loss and the association with threeâ€dimensional vortex ring formation in left ventricular inflow: In vivo evaluation using fourâ€dimensional flow MRI. Magnetic Resonance in Medicine, 2017, 77, 794-805.	3.0	92
60	Interâ€station intensity standardization for wholeâ€body <scp>MR</scp> data. Magnetic Resonance in Medicine, 2017, 77, 422-433.	3.0	11
61	Automated Ischemic Lesion Segmentation in MRI Mouse Brain Data after Transient Middle Cerebral Artery Occlusion. Frontiers in Neuroinformatics, 2017, 11, 3.	2.5	27
62	Detection of Conversion from Mild Cognitive Impairment to Alzheimer's Disease Using Longitudinal Brain MRI. Frontiers in Neuroinformatics, 2017, 11, 16.	2.5	26
63	MRI Mouse Brain Data of Ischemic Lesion after Transient Middle Cerebral Artery Occlusion. Frontiers in Neuroinformatics, 2017, 11, 51.	2.5	9
64	Co-expression Patterns between ATN1 and ATXN2 Coincide with Brain Regions Affected in Huntington's Disease. Frontiers in Molecular Neuroscience, 2017, 10, 399.	2.9	9
65	Tissue characterization with depth-resolved attenuation coefficient and backscatter term in in intravascular optical coherence tomography images. Journal of Biomedical Optics, 2017, 22, 1.	2.6	42
66	Validation of full-field optical coherence tomography in distinguishing malignant and benign tissue in resected pancreatic cancer specimens. PLoS ONE, 2017, 12, e0175862.	2.5	18
67	EpCAM as multi-tumour target for near-infrared fluorescence guided surgery. BMC Cancer, 2016, 16, 884.	2.6	36
68	Analysis and compensation for the effect of the catheter position on image intensities in intravascular optical coherence tomography. Journal of Biomedical Optics, 2016, 21, 126005.	2.6	5
69	Hierarchical Stochastic Neighbor Embedding. Computer Graphics Forum, 2016, 35, 21-30.	3.0	103
70	Noninvasive Detection of Metastases and Follicle Density in Ovarian Tissue Using Full-Field Optical Coherence Tomography. Clinical Cancer Research, 2016, 22, 5506-5513.	7.0	26
71	Mass Cytometry of the Human Mucosal Immune System Identifies Tissue- and Disease-Associated Immune Subsets. Immunity, 2016, 44, 1227-1239.	14.3	139
72	Cytosplore: Interactive Immune Cell Phenotyping for Large Singleâ€Cell Datasets. Computer Graphics Forum, 2016, 35, 171-180.	3.0	108

#	Article	IF	CITATIONS
73	Data-driven identification of prognostic tumor subpopulations using spatially mapped t-SNE of mass spectrometry imaging data. Proceedings of the National Academy of Sciences of the United States of America, 2016, 113, 12244-12249.	7.1	154
74	Automatic aortic root segmentation in CTA whole-body dataset. , 2016, , .		1
75	Fast Automatic Step Size Estimation for Gradient Descent Optimization of Image Registration. IEEE Transactions on Medical Imaging, 2016, 35, 391-403.	8.9	36
76	Fusion of CTA and XA data using 3D centerline registration for plaque visualization during coronary intervention. , 2016, , .		1
77	Improved selection of cortical ovarian strips for autotransplantation of ovarian tissue using full-field optical coherence tomography (FFOCT). , 2016, , .		0
78	Genome-wide coexpression of steroid receptors in the mouse brain: Identifying signaling pathways and functionally coordinated regions. Proceedings of the National Academy of Sciences of the United States of America, 2016, 113, 2738-2743.	7.1	73
79	Gene co-expression analysis identifies brain regions and cell types involved in migraine pathophysiology: a GWAS-based study using the Allen Human Brain Atlas. Human Genetics, 2016, 135, 425-439.	3.8	47
80	Light intensity matching between different intravascular optical coherence tomography systems. Proceedings of SPIE, 2016, , .	0.8	2
81	Morphological maturation of the mouse brain: An in vivo MRI and histology investigation. NeuroImage, 2016, 125, 144-152.	4.2	120
82	Accuracy Estimation for Medical Image Registration Using Regression Forests. Lecture Notes in Computer Science, 2016, , 107-115.	1.3	16
83	Super-resolution reconstruction of late gadolinium-enhanced MRI for improved myocardial scar assessment. Journal of Magnetic Resonance Imaging, 2015, 42, 160-167.	3.4	14
84	Segmentation of branching vascular structures using adaptive subdivision surface fitting. Proceedings of SPIE, 2015, , .	0.8	11
85	Automated extraction and labelling of the arterial tree from whole-body MRA data. Medical Image Analysis, 2015, 24, 28-40.	11.6	8
86	Optical Mammography Using Diffuse Optical Spectroscopy for Monitoring Tumor Response to Neoadjuvant Chemotherapy in Women with Locally Advanced Breast Cancer. Clinical Cancer Research, 2015, 21, 577-584.	7.0	32
87	Early identification of non-responding locally advanced breast tumors receiving neoadjuvant chemotherapy. , 2015, , .		1
88	Fast linear geodesic shape regression using coupled logdemons registration. , 2015, , .		2
89	Probabilistic atlas based labeling of the cerebral vessel tree. Proceedings of SPIE, 2015, , .	0.8	2
90	Fluorescence lifetime imaging to differentiate bound from unbound ICG-cRGD both <i>in vivo</i> . Proceedings of SPIE, 2015, , .	0.8	5

#	Article	IF	CITATIONS
91	Characterization and Evaluation of the Artemis Camera for Fluorescence-Guided Cancer Surgery. Molecular Imaging and Biology, 2015, 17, 413-423.	2.6	37
92	Hi-C Chromatin Interaction Networks Predict Co-expression in the Mouse Cortex. PLoS Computational Biology, 2015, 11, e1004221.	3.2	45
93	Repeatability of in vivo quantification of atherosclerotic carotid artery plaque components by supervised multispectral classification. Magnetic Resonance Materials in Physics, Biology, and Medicine, 2015, 28, 535-545.	2.0	16
94	Detection of Alzheimer's disease using group lasso SVM-based region selection. Proceedings of SPIE, 2015, , .	0.8	1
95	Respiratory motion estimation in x-ray angiography for improved guidance during coronary interventions. Physics in Medicine and Biology, 2015, 60, 3617-3637.	3.0	11
96	Shared Pathways Among Autism Candidate Genes Determined by Co-expression Network Analysis of the Developing Human Brain Transcriptome. Journal of Molecular Neuroscience, 2015, 57, 580-594.	2.3	54
97	Interactive analysis of geographically distributed population imaging data collections over light-path data networks. Proceedings of SPIE, 2015, , .	0.8	0
98	Hierarchical Shape Distributions for Automatic Identification of 3D Diastolic Vortex Rings from 4D Flow MRI. Lecture Notes in Computer Science, 2015, , 467-475.	1.3	2
99	Evaluating intensity normalization for multispectral classification of carotid atherosclerotic plaque. , 2015, , .		0
100	Visualizing the spatial gene expression organization in the brain through non-linear similarity embeddings. Methods, 2015, 73, 79-89.	3.8	54
101	A Stochastic Quasi-Newton Method for Non-Rigid Image Registration. Lecture Notes in Computer Science, 2015, , 297-304.	1.3	5
102	Fast automatic estimation of the optimization step size for nonrigid image registration. , 2014, , .		2
103	Automatic registration of imaging mass spectrometry data to the Allen Brain Atlas transcriptome. , 2014, , .		2
104	Genomic connectivity networks based on the BrainSpan atlas of the developing human brain. , 2014, , .		1
105	Brain maturation of the adolescent rat cortex and striatum: Changes in volume and myelination. NeuroImage, 2014, 84, 35-44.	4.2	113
106	Evaluation of automated statistical shape model based knee kinematics from biplane fluoroscopy. Journal of Biomechanics, 2014, 47, 122-129.	2.1	34
107	Vortex flow during early and late left ventricular filling in normal subjects: quantitative characterization using retrospectively-gated 4D flow cardiovascular magnetic resonance and three-dimensional vortex core analysis. Journal of Cardiovascular Magnetic Resonance, 2014, 16, 78.	3.3	118
108	Additional Diagnostic Value of Integrated Analysis of Cardiac CTA and SPECT MPI Using the SMARTVis System in Patients with Suspected Coronary Artery Disease. Journal of Nuclear Medicine, 2014, 55, 50-57.	5.0	18

4

#	Article	IF	CITATIONS
109	Automatic Generic Registration of Mass Spectrometry Imaging Data to Histology Using Nonlinear Stochastic Embedding. Analytical Chemistry, 2014, 86, 9204-9211.	6.5	62
110	Automatic Registration of Mass Spectrometry Imaging Data Sets to the Allen Brain Atlas. Analytical Chemistry, 2014, 86, 3947-3954.	6.5	58
111	Interactive Local Super-Resolution Reconstruction of Whole-Body MRI Mouse Data: A Pilot Study with Applications to Bone and Kidney Metastases. PLoS ONE, 2014, 9, e108730.	2.5	3
112	Automated algorithm for reconstruction of the complete spine from multistation 7T MR data. Magnetic Resonance in Medicine, 2013, 69, 1777-1786.	3.0	10
113	Comparative exploration of whole-body MR through locally rigid transforms. International Journal of Computer Assisted Radiology and Surgery, 2013, 8, 635-647.	2.8	5
114	Automatic quantification and characterization of coronary atherosclerosis with computed tomography coronary angiography: cross-correlation with intravascular ultrasound virtual histology. International Journal of Cardiovascular Imaging, 2013, 29, 1177-1190.	1.5	178
115	Statistical coronary motion models for 2D+t/3D registration of X-ray coronary angiography and CTA. Medical Image Analysis, 2013, 17, 698-709.	11.6	42
116	Automated registration of multispectral MR vessel wall images of the carotid artery. Medical Physics, 2013, 40, 121904.	3.0	18
117	Deformation texture-based features for classification in Alzheimer's disease. , 2013, , .		2
118	A visualization platform for high-throughput, follow-up, co-registered multi-contrast MRI rat brain data. , 2013, , .		2
119	Model-based alignment of Look-Locker MRI sequences for calibrated myocardical scar tissue quantification. , 2013, , .		4
120	Fast parallel image registration on CPU and GPU for diagnostic classification of Alzheimer's disease. Frontiers in Neuroinformatics, 2013, 7, 50.	2.5	359
121	Improved Myocardial Scar Characterization by Super-Resolution Reconstruction in Late Gadolinium Enhanced MRI. Lecture Notes in Computer Science, 2013, 16, 147-154.	1.3	2
122	Joint Intensity Inhomogeneity Correction for Whole-Body MR Data. Lecture Notes in Computer Science, 2013, 16, 106-113.	1.3	3
123	CT-based handling and analysis of preclinical multimodality imaging data of bone metastases. BoneKEy Reports, 2012, 1, 79.	2.7	2
124	Regression-Based Cardiac Motion Prediction From Single-Phase CTA. IEEE Transactions on Medical Imaging, 2012, 31, 1311-1325.	8.9	21
125	Statistical Shape Model-Based Femur Kinematics From Biplane Fluoroscopy. IEEE Transactions on Medical Imaging, 2012, 31, 1573-1583.	8.9	21

126 Super-resolution reconstruction of whole-body MRI mouse data: An interactive approach. , 2012, , .

#	Article	IF	CITATIONS
127	Automated Bone Volume and Thickness Measurements in Small Animal Whole-Body MicroCT Data. Molecular Imaging and Biology, 2012, 14, 420-430.	2.6	13
128	Comprehensive visualization of multimodal cardiac imaging data for assessment of coronary artery disease: first clinical results of the SMARTVis tool. International Journal of Computer Assisted Radiology and Surgery, 2012, 7, 557-571.	2.8	12
129	Cardiac MR perfusion image processing techniques: A survey. Medical Image Analysis, 2012, 16, 767-785.	11.6	33
130	Fully Automated Attenuation Measurement and Motion Correction in FLIP Image Sequences. IEEE Transactions on Medical Imaging, 2012, 31, 461-473.	8.9	7
131	Segmentation and Visual Analysis of Whole-Body Mouse Skeleton microSPECT. PLoS ONE, 2012, 7, e48976.	2.5	11
132	Robust Motion Correction in the Frequency Domain of Cardiac MR Stress Perfusion Sequences. Lecture Notes in Computer Science, 2012, 15, 667-674.	1.3	4
133	Atlas-based articulated skeleton segmentation of μSPECT mouse data. , 2011, , .		1
134	Optical advances in skeletal imaging applied to bone metastases. Bone, 2011, 48, 106-114.	2.9	30
135	2D–3D shape reconstruction of the distal femur from stereo X-ray imaging using statistical shape models. Medical Image Analysis, 2011, 15, 840-850.	11.6	139
136	Articulated Whole-Body Atlases for Small Animal Image Analysis: Construction and Applications. Molecular Imaging and Biology, 2011, 13, 898-910.	2.6	29
137	Automated regional wall motion abnormality detection by combining rest and stress cardiac MRI: Correlation with contrastâ€enhanced MRI. Journal of Magnetic Resonance Imaging, 2011, 34, 270-278.	3.4	8
138	Towards integrated analysis of longitudinal whole-body small animal imaging studies. , 2011, , .		1
139	A patient-specific visualization tool for comprehensive analysis of coronary CTA and perfusion MRI data. Proceedings of SPIE, 2011, , .	0.8	1
140	Trends in Bioimaging and Signal Processing [In the Spotlight]. IEEE Signal Processing Magazine, 2011, 28, 200-191.	5.6	1
141	Automated Registration of Whole-Body Follow-Up MicroCT Data of Mice. Lecture Notes in Computer Science, 2011, 14, 516-523.	1.3	23
142	Comparison of Shape Regression Methods under Landmark Position Uncertainty. Lecture Notes in Computer Science, 2011, 14, 434-441.	1.3	7
143	Slice-Based Combination of Rest and Dobutamine–Stress Cardiac MRI Using a Statistical Motion Model to Identify Myocardial Infarction: Validation against Contrast-Enhanced MRI. Lecture Notes in Computer Science, 2011, , 267-274.	1.3	0
144	Atlas-based whole-body segmentation of mice from low-contrast Micro-CT data. Medical Image Analysis, 2010, 14, 723-737.	11.6	84

#	Article	IF	CITATIONS
145	Model driven quantification of left ventricular function from sparse single-beat 3D echocardiography. Medical Image Analysis, 2010, 14, 582-593.	11.6	16
146	Confidence of model based shape reconstruction from sparse data. , 2010, , .		8
147	Correspondence free 3D statistical shape model fitting to sparse x-ray projections. , 2010, , .		4
148	Fully Automatic Registration and Segmentation of First-Pass Myocardial Perfusion MR Image Sequences. Academic Radiology, 2010, 17, 1375-1385.	2.5	18
149	Articulated Planar Reformation for Change Visualization in Small Animal Imaging. IEEE Transactions on Visualization and Computer Graphics, 2010, 16, 1396-1404.	4.4	22
150	Atlas-based organ & bone approximation for ex-vivo μMRI mouse data: A pilot study. , 2010, , .		4
151	Conditional Shape Models for Cardiac Motion Estimation. Lecture Notes in Computer Science, 2010, 13, 452-459.	1.3	9
152	Identification of cellular dynamic patterns resulting from repetitive photobleaching using Independent Component Analysis. , 2009, , .		1
153	Atlas-driven scan planning for high-resolution micro-SPECT data acquisition based on multi-view photographs: a pilot study. , 2009, , .		7
154	Model driven quantification of left ventricular function from sparse single-beat 3D echocardiography. Proceedings of SPIE, 2009, , .	0.8	3
155	Automated Detection of Regional Wall Motion Abnormalities Based on a Statistical Model Applied to Multislice Short-Axis Cardiac MR Images. IEEE Transactions on Medical Imaging, 2009, 28, 595-607.	8.9	77
156	Automated left ventricular delineation in X-ray angiograms: A validation study. Catheterization and Cardiovascular Interventions, 2009, 73, 231-240.	1.7	4
157	2D/3D registration of micro-CT data to multi-view photographs based on a 3D distance map. , 2009, , .		11
158	Left Ventricle Segmentation from Contrast Enhanced Fast Rotating Ultrasound Images Using Three Dimensional Active Shape Models. Lecture Notes in Computer Science, 2009, , 295-302.	1.3	10
159	Information Processing in Medical Imaging 2007. Medical Image Analysis, 2008, 12, 729-730.	11.6	4
160	A 3-D Active Shape Model Driven by Fuzzy Inference: Application to Cardiac CT and MR. IEEE Transactions on Information Technology in Biomedicine, 2008, 12, 595-605.	3.2	74
161	Guest Editorial Functional Imaging of the Heart. IEEE Transactions on Medical Imaging, 2008, 27, 1545-1547.	8.9	0
162	Fully Automated Motion Correction in First-Pass Myocardial Perfusion MR Image Sequences. IEEE Transactions on Medical Imaging, 2008, 27, 1611-1621.	8.9	79

#	Article	IF	CITATIONS
163	Organ approximation in μCT data with low soft tissue contrast using an articulated whole-body atlas. , 2008, , .		12
164	FULLY AUTOMATED WHOLE-BODY REGISTRATION IN MICE USING AN ARTICULATED SKELETON ATLAS. , 2007, , .		19
165	Fully automatic estimation of object pose for segmentation initialization: application to cardiac MR and echocardiography images. , 2007, 6512, 1196.		3
166	Automated Contour Detection in Cardiac MRI Using Active Appearance Models. Investigative Radiology, 2007, 42, 697-703.	6.2	13
167	Special issue on functional imaging of the heart. IEEE Transactions on Medical Imaging, 2007, 26, 891-891.	8.9	0
168	Integrated visualization of multi-angle bioluminescence imaging and micro CT. , 2007, , .		6
169	Automated contour detection in X-ray left ventricular angiograms using multiview active appearance models and dynamic programming. IEEE Transactions on Medical Imaging, 2006, 25, 1158-1171.	8.9	29
170	An Integrated Automated Analysis Method for Quantifying Vessel Stenosis and Plaque Burden From Carotid MRI Images. Stroke, 2006, 37, 2162-2164.	2.0	32
171	Time Continuous Tracking and Segmentation of Cardiovascular Magnetic Resonance Images Using Multidimensional Dynamic Programming. Investigative Radiology, 2006, 41, 52-62.	6.2	61
172	Analysis of first-pass myocardial perfusion MRI using independent component analysis. , 2006, 6144, 596.		3
173	SPASM: A 3D-ASM for segmentation of sparse and arbitrarily oriented cardiac MRI data. Medical Image Analysis, 2006, 10, 286-303.	11.6	194
174	Automatic vessel wall contour detection and quantification of wall thickness in in-vivo MR images of the human aorta. Journal of Magnetic Resonance Imaging, 2006, 24, 595-602.	3.4	36
175	Automated quantification of cardiac short-axis multi-slice CT images for assessment of left ventricular global function. , 2005, , .		0
176	Multiview Active Appearance Models for Simultaneous Segmentation of Cardiac 2- and 4-Chamber Long-Axis Magnetic Resonance Images. Investigative Radiology, 2005, 40, 195-203.	6.2	18
177	Automated Segmentation of X-ray Left Ventricular Angiograms Using Multi-View Active Appearance Models and Dynamic Programming. Lecture Notes in Computer Science, 2005, , 23-32.	1.3	5
178	Influence of positional and angular variation of automatically planned short-axis stacks on quantification of left ventricular dimensions and function with cardiovascular magnetic resonance. Journal of Magnetic Resonance Imaging, 2005, 22, 754-764.	3.4	3
179	Accuracy of short-axis cardiac MRI automatically derived from scout acquisitions in free-breathing and breath-holding modes. Magnetic Resonance Materials in Physics, Biology, and Medicine, 2005, 18, 7-18.	2.0	12
180	Statistical Modeling and Segmentation in Cardiac MRI Using a Grid Computing Approach. Lecture Notes in Computer Science, 2005, , 6-15.	1.3	3

#	Article	IF	CITATIONS
181	Operator Induced Variability in Cardiovascular MR: Left Ventricular Measurements and Their Reproducibility. Journal of Cardiovascular Magnetic Resonance, 2005, 7, 447-457.	3.3	68
182	SPASM: Segmentation of Sparse and Arbitrarily Oriented Cardiac MRI Data Using a 3D-ASM. Lecture Notes in Computer Science, 2005, , 33-43.	1.3	6
183	Computer-aided diagnosis via model-based shape analysis. Academic Radiology, 2005, 12, 358-367.	2.5	34
184	3D Model-Based Approach to Lung Registration and Prediction of Respiratory Cardiac Motion. Lecture Notes in Computer Science, 2005, 8, 951-959.	1.3	4
185	Cardiovascular MR Image Analysis. , 2005, , 193-239.		Ο
186	Evaluation of a New Method for Automated Detection of Left Ventricular Boundaries in Time Series of Magnetic Resonance Images Using an Active Appearance Motion Model. Journal of Cardiovascular Magnetic Resonance, 2004, 6, 609-617.	3.3	50
187	Automatic plaque characterization and vessel wall segmentation in magnetic resonance images of atherosclerotic carotid arteries. , 2004, , .		7
188	Towards 'One-Stop' Cardiac MR Image Analysis. Imaging Decisions (Berlin, Germany), 2004, 8, 2-12.	0.2	1
189	Automatic segmentation and plaque characterization in atherosclerotic carotid artery MR images. Magnetic Resonance Materials in Physics, Biology, and Medicine, 2004, 16, 227-234.	2.0	127
190	Automated Short-Axis Cardiac Magnetic Resonance Image Acquisitions. Investigative Radiology, 2004, 39, 747-755.	6.2	6
191	Computer-aided diagnosis via model-based shape analysis: cardiac MR and echo. International Congress Series, 2003, 1256, 1013-1018.	0.2	5
192	Multi-view active appearance models for consistent segmentation of multiple standard views: application to long- and short-axis cardiac MR images. International Congress Series, 2003, 1256, 1141-1146.	0.2	21
193	Independent component analysis in statistical shape models. , 2003, , .		27
194	Left ventricle contour detection in x-ray angiograms using multi-view active appearance models. , 2003, 5032, 394.		7
195	Disease characterization of active appearance model coefficients. , 2003, , .		2
196	Automated classification of wall motion abnormalities by principal component analysis of endocardial shape motion patterns in echocardiograms. , 2003, , .		3
197	Three-dimensional active shape model matching for left ventricle segmentation in cardiac CT. , 2003, , .		3
198	Segmentation of cardiac MR volume data using 3D active appearance models. , 2002, , .		12

BOUDEWIJN P F LELIEVELDT

#	Article	IF	CITATIONS
199	Automatic segmentation of echocardiographic sequences by active appearance motion models. IEEE Transactions on Medical Imaging, 2002, 21, 1374-1383.	8.9	257
200	3-D active appearance models: segmentation of cardiac MR and ultrasound images. IEEE Transactions on Medical Imaging, 2002, 21, 1167-1178.	8.9	348
201	Optimal design of radial basis function neural networks for fuzzy-rule extraction in high dimensional data. Pattern Recognition, 2002, 35, 659-675.	8.1	39
202	Fully automated endocardial contour detection in time sequences of echocardiograms by three-dimensional active appearance models. , 2002, , .		7
203	Active Appearance–Motion Models for fully automated endocardial contour detection in time sequences of echocardiograms. International Congress Series, 2001, 1230, 941-947.	0.2	4
204	Time continuous segmentation of cardiac MR images using Active Appearance Motion Models. International Congress Series, 2001, 1230, 961-966.	0.2	6
205	Multistage hybrid active appearance model matching: segmentation of left and right ventricles in cardiac MR images. IEEE Transactions on Medical Imaging, 2001, 20, 415-423.	8.9	290
206	Neuro-fuzzy systems for computer-aided myocardial viability assessment. IEEE Transactions on Medical Imaging, 2001, 20, 1302-1313.	8.9	24
207	<title>Time-continuous segmentation of cardiac MR image sequences using active appearance motion models</title> ., 2001, , .		17
208	<title>Active appearance motion models for endocardial contour detection in time sequences of echocardiograms</title> ., 2001,,.		13
209	Myocardium extraction in positron emission tomography based on soft computing. Computerized Medical Imaging and Graphics, 2001, 25, 277-286.	5.8	4
210	Automated Observer-independent Acquisition of Cardiac Short-Axis MR Images: A Pilot Study. Radiology, 2001, 221, 537-542.	7.3	39
211	A Virtual Exploring Robot for Adaptive Left Ventricle Contour Detection in Cardiac MR Images. Lecture Notes in Computer Science, 2001, , 1287-1288.	1.3	1
212	Time-Continuous Segmentation of Cardiac Image Sequences Using Active Appearance Motion Models. Lecture Notes in Computer Science, 2001, , 446-452.	1.3	26
213	<title>Segmentation of cardiac MR images: an active appearance model approach</title> . , 2000, 3979, 224.		18
214	Quantification of Global and Regional Ventricular Function in Cardiac Magnetic Resonance Imaging. Topics in Magnetic Resonance Imaging, 2000, 11, 348-358.	1.2	16
215	Anatomical Modeling with Fuzzy Implicit Surface Templates: Application to Automated Localization of the Heart and Lungs in Thoracic MR Volumes. Computer Vision and Image Understanding, 2000, 80, 1-20.	4.7	15
216	A neuro-fuzzy system for automatic assessment of myocardial viability in positron emission tomography. , 2000, , .		0

13

#	Article	IF	CITATIONS
217	A multiresolution image segmentation technique based on pyramidal segmentation and fuzzy clustering. IEEE Transactions on Image Processing, 2000, 9, 1238-1248.	9.8	126
218	Fuzzy feature selection. Pattern Recognition, 1999, 32, 2011-2019.	8.1	44
219	Anatomical model matching with fuzzy implicit surfaces for segmentation of thoracic volume scans. IEEE Transactions on Medical Imaging, 1999, 18, 218-230.	8.9	43
220	Anatomical Modeling with Fuzzy Implicit Surfaces: Application to Automated Localization of the Heart and Lungs in Thoracic MR Images. Lecture Notes in Computer Science, 1999, , 400-405.	1.3	0
221	A new cluster validity index for the fuzzy c-mean. Pattern Recognition Letters, 1998, 19, 237-246.	4.2	337
222	A virtual exploring mobile robot for left ventricle contour tracking. , 0, , .		3
223	Model driven interpretation of velocity encoded aortic flow images by means of Voronoi arrangement matrices. , 0, , .		0
224	Automated model driven localization of the heart and lung surfaces in thoracic MR images. , 0, , .		1
225	Fully automated endocardial contour detection in time sequences of echocardiograms by active appearance motion models. , 0, , .		4
226	Active appearance motion model segmentation. , 0, , .		6
227	Efficient Reconstruction of Cardiac LV Surfaces Using a 3D Sparse ASM. , 0, , .		0
228	Identification of a Disease-Associated Network of Intestinal Immune Cells in Treatment-Naive Inflammatory Bowel Disease. Frontiers in Immunology, 0, 13, .	4.8	7